



A CFD study of hygro-thermal stresses distribution in tubular-shaped ambient air-breathing PEM micro fuel cell during regular cell operation

Maher A.R. Sadiq Al-Baghdadi

Fuel Cell Research Center, International Energy & Environment Foundation, Al-Najaf, P.O.Box 39, Iraq.

Abstract

The need for improved lifetime of air-breathing proton exchange membrane (PEM) fuel cells for portable applications necessitates that the failure mechanisms be clearly understood and life prediction models be developed, so that new designs can be introduced to improve long-term performance. An operating air-breathing PEM fuel cell has varying local conditions of temperature, humidity. As a result of in the changes in temperature and moisture, the membrane, GDL and bipolar plates will all experience expansion and contraction. Because of the different thermal expansion and swelling coefficients between these materials, hygro-thermal stresses are introduced into the unit cell during operation. In addition, the non-uniform current and reactant flow distributions in the cell result in non-uniform temperature and moisture content of the cell which could in turn, potentially causing localized increases in the stress magnitudes, and this leads to mechanical damage, which can appear as through-the-thickness flaws or pinholes in the membrane, or delaminating between the polymer membrane and gas diffusion layers. Therefore, in order to acquire a complete understanding of these damage mechanisms in the membranes and gas diffusion layers, mechanical response under steady-state hygro-thermal stresses should be studied under real cell operation conditions.

A three-dimensional, multi-phase, non-isothermal computational fluid dynamics model of a novel, tubular, ambient air-breathing, proton exchange membrane micro fuel cell has been developed and used to investigate the displacement, deformation, and stresses inside the whole cell, which developed during the cell operation due to the changes of temperature and relative humidity. The behaviour of the fuel cell during operation has been studied and investigated under real cell operating conditions. In addition to the new and complex geometry, a unique feature of the present model is to incorporate the effect of mechanical, hygro and thermal stresses into actual three-dimensional fuel cell model. The results show that the non-uniform distribution of stresses, caused by the temperature gradient in the cell, induces localized bending stresses, which can contribute to delaminating between the membrane and the gas diffusion layers. The non-uniform distribution of stresses can also contribute to delaminating between the gas diffusion layers and the current collectors. These stresses may explain the occurrence of cracks and pinholes in the fuel cells components under steady-state loading during regular cell operation, especially in the high loading conditions.

Copyright © 2010 International Energy and Environment Foundation - All rights reserved.

Keywords: Ambient air-breathing, PEM fuel cell, CFD, Hygro-Thermal stresses, Nafion.

1. Introduction

Fuel cell system is an advanced power system for the future that is sustainable, clean and environmental friendly. Small fuel cells have provided significant advantages in portable electronic applications over conventional battery systems. Competitive costs, instant recharge, and high energy density make fuel cells ideal for supplanting batteries in portable electronic devices. However, the typical PEM fuel cell system with its heavy reliance on subsystems for cooling, humidification and air supply would not be practical in small applications. The air-breathing PEM fuel cells without moving parts (external humidification instrument, fans or pumps) are one of the most competitive candidates for future portable-power applications. In air-breathing PEM fuel cell, the cathode side of the cell is directly open to ambient air. The oxygen needed by the fuel cell electrochemical reaction is taken directly from the surrounding air by natural convection and diffusion through the gas diffusion backing into the cathode electrode.

It has been known that the oxygen transport limitation plays a great role in the performance of air-breathing fuel cells from literatures [1-4]. The current production by electrochemical reaction is directly proportional to the local oxygen concentration in the fuel cell. Inadequate airflow in the planar air-breathing PEM fuel cell cannot provide enough oxygen for the electrochemical reaction on the active surfaces under the land areas. It results in heterogeneous current distribution in the electrode that reduces the performance of the fuel cell. Thus, one of the greater challenges in the design of passive fuel cells is how to provide enough oxygen for the electrochemical reaction on the entire active surface.

One of the new architectures in PEM fuel cell design is a tubular-shaped fuel cell. Fuel cell companies and research institutes may have carried out various systematic experimental studies for this type of the fuel cell, for different specific purposes, but most the data would be proprietary in nature and very limited data are available in the open literature. There are several reasons that make the tubular design more advantageous than the planar one for medium to high power stacks: (i) elimination of the flow field: lower pressure drop at the anode fields and no time-consuming machinery due to shorter flow fields, (ii) uniform pressure applied to the MEA by the cathode, (iii) quicker response when switching from fuel cell mode to electrolyser mode in a unitized regenerative fuel cell, (iv) greater cathode surface that increases the amount of oxygen reduction, the rate of which is slower than the hydrogen oxidation rate. In addition, (v) tubular designs can achieve much higher active area to volume ratios, and hence higher volumetric power densities.

For portable applications like laptops, camcorders, and mobile phones the requirements of the fuel cell systems are even more specific than for stationary and vehicular applications. The requirements for portable applications are mostly focused on lifetime, size and weight of the system as well as the temperature. The need for improved lifetime of air-breathing proton exchange membrane (PEM) fuel cells necessitates that the failure mechanisms be clearly understood and life prediction models be developed, so that new designs can be introduced to improve long-term performance. Durability is a complicated phenomenon, linked to the chemical and mechanical interactions of the fuel cell components, i.e. electrocatalysts, membranes, gas diffusion layers, and bipolar plates, under severe environmental conditions, such as elevated temperature and low humidity [5, 6]. In fuel cell systems, failure may occur in several ways such as chemical degradation of the ionomer membrane or mechanical failure in the PEM that results in gradual reduction of ionic conductivity, increase in the total cell resistance, and the reduction of voltage and loss of output power [7]. Mechanical damage in the PEM can appear as through-the-thickness flaws or pinholes in the membrane, or delaminating between the polymer membrane and gas diffusion layers [8]. An operating fuel cell has varying local conditions of temperature, humidity. As a result of in the changes in temperature and moisture, the membrane, GDL and bipolar plates will all experience expansion and contraction. Because of the different thermal expansion and swelling coefficients between these materials, hygro-thermal stresses are introduced into the unit cell during operation. In addition, the non-uniform current and reactant flow distributions in the cell result in non-uniform temperature and moisture content of the cell which could in turn, potentially causing localized increases in the stress magnitudes, and this leads to mechanical damage, which can appear as through-the-thickness flaws or pinholes in the membrane, or delaminating between the polymer membrane and gas diffusion layers [9, 10]. Therefore, in order to acquire a complete understanding of these damage mechanisms in the membranes, mechanical response under steady-state hygro-thermal stresses should be studied under real cell operation conditions [11, 12]. The development of physically representative models that allow reliable simulation of the processes under realistic conditions is essential to the development and optimization of fuel cells, improve long-term performance, the introduction of cheaper materials and fabrication techniques, and the design and development of

novel architectures. The difficult experimental environment of fuel cell systems has stimulated efforts to develop models that could simulate and predict multi-dimensional coupled transport of reactants, heat and charged species using computational fluid dynamic (CFD) methods. The strength of the CFD numerical approach is in providing detailed insight into the various transport mechanisms and their interaction, and in the possibility of performing parameters sensitivity analyses.

An operating fuel cell has varying local conditions of temperature, humidity, and power generation (and thereby heat generation) across the active area of the fuel cell in three-dimensions. Nevertheless, no models have yet been published to incorporate the effect of hygro-thermal stresses into actual fuel cell models to study the effect of these real conditions on the stresses developed in the complete cell. In this work, a three-dimensional, multi-phase, CFD model of a novel tubular geometry air-breathing PEM micro fuel cell has been developed and used to investigate the displacement, deformation, and stresses inside the cell during the cell operation under real cell operating conditions.

2. Model description

The present work presents a comprehensive three-dimensional, multi-phase, non-isothermal model of a tubular-shaped ambient air-breathing PEM micro fuel cell that incorporates the significant physical processes and the key parameters affecting fuel cell performance. The following assumptions are made: (i.) the fuel cell operates under steady-state conditions; (ii.) to alleviate the need for air distribution channels, along with the necessary pumps and fans, the cathode gas diffusion layer is in direct contact with the ambient air; (iii.) the ionic conductivity of the membrane is constant; (iv.) the membrane is impermeable to gases and cross-over of reactant gases is neglected; (v.) the gas diffusion layer is homogeneous and isotropic; (vi.) the flow in the natural convection region is laminar; (vii.) the produced water is in the vapour phase; (viii.) two-phase flow inside the porous media; (ix.) both phases occupy a certain local volume fraction inside the porous media and their interaction is accounted for through a multi-fluid approach; (x.) external humidification systems are eliminated and the fuel cell relies on the ambient relative humidity and water production in the cathode for the humidification of the membrane; (xi.) the circulating ambient air facilitates the cooling of the fuel cell in lieu of a dedicated heat management system.

The model accounts for both gas and liquid phase in the same computational domain, and thus allows for the implementation of phase change inside the gas diffusion layers. The model includes the transport of gaseous species, liquid water, protons, energy, and water dissolved in the ion-conducting polymer. Water transport inside the porous gas diffusion layer and catalyst layer is described by two physical mechanisms: viscous drag and capillary pressure forces, and is described by advection within the gas channel. Water transport across the membrane is also described by two physical mechanisms: electro-osmotic drag and diffusion. Water is assumed to be exchanged among three phases; liquid, vapour, and dissolved, and equilibrium among these phases is assumed.

In addition to the new and complex geometry, a unique feature of the present model is to incorporate the effect of hygro and thermal stresses into actual three-dimensional fuel cell model. This model also takes into account convection and diffusion of different species in the channel as well as in the porous gas diffusion layer, heat transfer in the solids as well as in the gases, and electrochemical reactions. The model reflects the influence of numerous parameters on fuel cell performance including geometry, materials, operating and others to investigate the in situ stresses in polymer membranes. The present multi-phase model is capable of identifying important parameters for the wetting behaviour of the gas diffusion layers and can be used to identify conditions that might lead to the onset of pore plugging, which has a detrimental effect of the fuel cell performance.

2.1 Computational domain

A schematic description of a tubular-shaped air-breathing PEM micro fuel cell is shown in Figure 1a. The cathode of the cell is directly open to ambient air. The oxygen needed by the fuel cell reaction is transferred by natural convection and diffusion through the gas diffusion backing into the cathode electrode. A computational model of an entire cell would require very large computing resources and excessively long simulation times. The computational domain in this study is therefore limited to one straight flow channel. The full computational domain consists of anode gas flow field, and the MEA is shown in Figure 1b.

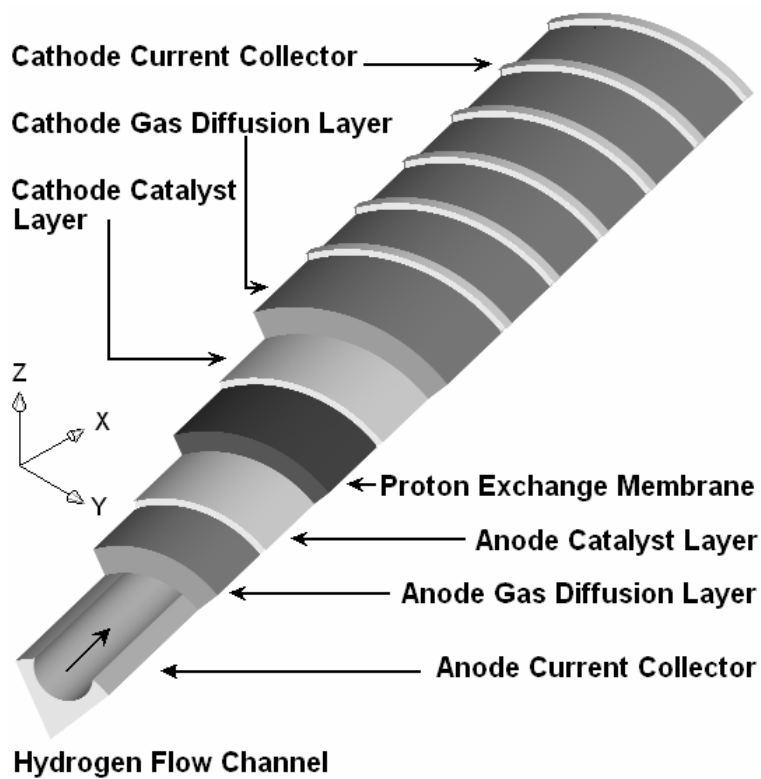
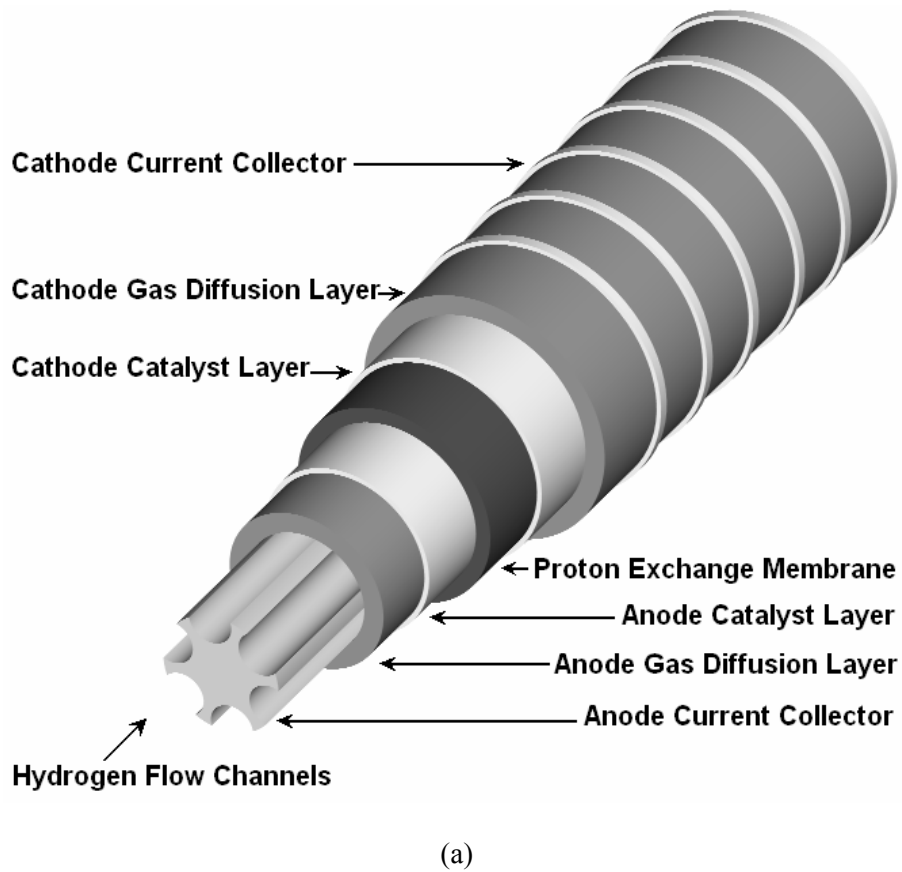


Figure 1. (a) Schematic of a tubular-shaped ambient air-breathing PEM micro fuel cell, and (b) three-dimensional computational domain

2.2 Model equations

2.2.1 Air and fuel gas flow

In natural convection region, the transport equations solved in the ambient air include continuity, momentum, energy and mass transport equations. In the fuel channel, the gas-flow field is obtained by solving the steady-state Navier-Stokes equations, i.e. the continuity equation, the mass conservation equation for each phase yields the volume fraction (r) and along with the momentum equations the pressure distribution inside the channel. The continuity equation for the gas phase inside the channel is given by;

$$\nabla \cdot (r_g \rho_g \mathbf{u}_g) = 0 \quad (1)$$

and for the liquid phase inside the channel becomes;

$$\nabla \cdot (r_l \rho_l \mathbf{u}_l) = 0 \quad (2)$$

where \mathbf{u} is velocity vector (m/s), ρ is density (kg/m³). Subscript (g) is a gas phase and (l) is a liquid phase.

Two sets of momentum equations are solved in the channel, and they share the same pressure field. Under these conditions, it can be shown that the momentum equations becomes;

$$\nabla \cdot (\rho_g \mathbf{u}_g \otimes \mathbf{u}_g - \mu_g \nabla \mathbf{u}_g) = -\nabla r_g \left(P + \frac{2}{3} \mu_g \nabla \cdot \mathbf{u}_g \right) + \nabla \cdot [\mu_g (\nabla \mathbf{u}_g)^T] \quad (3)$$

$$\nabla \cdot (\rho_l \mathbf{u}_l \otimes \mathbf{u}_l - \mu_l \nabla \mathbf{u}_l) = -\nabla r_l \left(P + \frac{2}{3} \mu_l \nabla \cdot \mathbf{u}_l \right) + \nabla \cdot [\mu_l (\nabla \mathbf{u}_l)^T] \quad (4)$$

where P is pressure (Pa), μ is viscosity [kg/(m·s)].

The mass balance is described by the divergence of the mass flux through diffusion and convection. Multiple species are considered in the gas phase only, and the species conservation equation in multi-component, multi-phase flow can be written in the following expression for species i ;

$$\nabla \cdot \left[-r_g \rho_g y_i \sum_{j=1}^N D_{ij} \frac{M}{M_j} \left[\left(\nabla y_j + y_j \frac{\nabla M}{M} \right) + (x_j - y_j) \frac{\nabla P}{P} \right] + r_g \rho_g y_i \cdot \mathbf{u}_g + D_i^T \frac{\nabla T}{T} \right] = 0 \quad (5)$$

where T is temperature (K), y is mass fraction, x is mole fraction. Subscript i denotes oxygen at the cathode side and hydrogen at the anode side, and j is water vapour in both cases. Nitrogen is the third species at the cathode side.

The Maxwell-Stefan diffusion coefficients of any two species are dependent on temperature and pressure. They can be calculated according to the empirical relation based on kinetic gas theory [13];

$$D_{ij} = \frac{T^{1.75} \times 10^{-3}}{P \left[\left(\sum_k V_{ki} \right)^{1/3} + \left(\sum_k V_{kj} \right)^{1/3} \right]^2} \left[\frac{1}{M_i} + \frac{1}{M_j} \right]^{1/2} \quad (6)$$

In this equation, pressure is in [atm] and the binary diffusion coefficient is in [cm²/s]. The values for $\left(\sum V_{ki} \right)$ are given by Fuller et al. [13].

The temperature field is obtained by solving the convective energy equation;

$$\nabla \cdot (r_g (\rho_g C_{p_g} \mathbf{u}_g T - k_g \nabla T)) = 0 \quad (7)$$

where C_{p_g} is a specific heat capacity (J/(kg·K)), and k_g is gases thermal conductivity (W/(m·K)).

The gas phase and the liquid phase are assumed to be in thermodynamic equilibrium; hence the temperature of the liquid water is the same as the gas phase temperature.

2.2.2 Gas diffusion layers

The physics of multiple phases through a porous medium is further complicated here with phase change and the sources and sinks associated with the electrochemical reaction. The equations used to describe

transport in the gas diffusion layers are given below. Mass transfer in the form of evaporation ($\dot{m}_{phase} > 0$) and condensation ($\dot{m}_{phase} < 0$) is assumed. Where \dot{m}_{phase} is mass transfer: for evaporation ($\dot{m}_{phase} = \dot{m}_{evap}$) and for condensation ($\dot{m}_{phase} = \dot{m}_{cond}$) (kg/s).

So that the mass balance equations for both phases are;

$$\nabla \cdot ((1 - sat)\rho_g \epsilon \mathbf{u}_g) = \dot{m}_{phase} \tag{8}$$

$$\nabla \cdot (sat \cdot \rho_l \epsilon \mathbf{u}_l) = \dot{m}_{phase} \tag{9}$$

where sat is saturation, ϵ is porosity.

The momentum equation for the gas phase reduces to Darcy's law, which is, however, based on the relative permeability for the gas phase (Kp). The relative permeability accounts for the reduction in pore space available for one phase due to the existence of the second phase [14, 15].

The momentum equation for the gas phase inside the gas diffusion layer becomes;

$$\mathbf{u}_g = -(1 - sat) \frac{Kp}{\mu_g} \nabla P \tag{10}$$

where Kp is hydraulic permeability (m^2).

Two liquid water transport mechanisms are considered; shear, which drags the liquid phase along with the gas phase in the direction of the pressure gradient, and capillary forces, which drive liquid water from high to low saturation regions [14, 15]. Therefore, the momentum equation for the liquid phase inside the gas diffusion layer becomes;

$$\mathbf{u}_l = -\frac{KP_l}{\mu_l} \nabla P + \frac{KP_l}{\mu_l} \frac{\partial P_c}{\partial sat} \nabla sat \tag{11}$$

where P_c is capillary pressure (Pa).

The functional variation of capillary pressure with saturation is calculated as follows [15];

$$P_c = \sigma \left(\frac{\epsilon}{KP} \right)^{1/2} (1.417(1 - sat) - 2.12(1 - sat)^2 + 1.263(1 - sat)^3) \tag{12}$$

where σ is surface tension (N/m).

The liquid phase consists of pure water, while the gas phase has multi components. The transport of each species in the gas phase is governed by a general convection-diffusion equation in conjunction which the Stefan-Maxwell equations to account for multi species diffusion;

$$\nabla \cdot \left[\begin{array}{c} -(1 - sat)\rho_g \epsilon y_i \sum_{j=1}^N D_{ij} \frac{M}{M_j} \left[\left(\nabla y_j + y_j \frac{\nabla M}{M} \right) + (x_j - y_j) \frac{\nabla P}{P} \right] + \\ (1 - sat)\rho_g \epsilon y_i \cdot \mathbf{u}_g + \epsilon D_i^T \frac{\nabla T}{T} \end{array} \right] = \dot{m}_{phase} \tag{13}$$

In order to account for geometric constraints of the porous media, the diffusivities are corrected using the Bruggemann correction formula [16];

$$D_{ij}^{eff} = D_{ij} \times \epsilon^{1.5} \tag{14}$$

The heat transfer in the gas diffusion layers is governed by the energy equation as follows;

$$\nabla \cdot ((1 - sat)\rho_g \epsilon Cp_g \mathbf{u}_g T - k_{eff,g} \epsilon \nabla T) = \epsilon \beta (T_{solid} - T) - \epsilon \dot{m}_{phase} \Delta H_{evap} \tag{15}$$

where k_{eff} is effective electrode thermal conductivity (W/m-K), the term ($\epsilon \beta (T_{solid} - T)$), on the right hand side, accounts for the heat exchange to and from the solid matrix of the GDL. β is a modified heat transfer coefficient that accounts for the convective heat transfer in [W/m^2] and the specific surface area [m^2/m^3] of the porous medium [17]. Hence, the unit of β is [W/m^3]. The gas phase and the liquid phase are assumed to be in thermodynamic equilibrium, i.e., the liquid water and the gas phase are at the same temperature.

The potential distribution in the gas diffusion layers is governed by;

$$\nabla \cdot (\lambda_e \nabla \phi) = 0 \quad (16)$$

where λ_e is electrode electronic conductivity (S/m).

In order to account for the magnitude of phase change inside the GDL, expressions are required to relate the level of over- and undersaturation as well as the amount of liquid water present to the amount of water undergoing phase change. In the present work, the procedure of Berning and Djilali [15] was used to account for the magnitude of phase change inside the GDL.

2.2.3 Catalyst layers

The catalyst layer is treated as a thin interface, where sink and source terms for the reactants are implemented. Due to the infinitesimal thickness, the source terms are actually implemented in the last grid cell of the porous medium. At the cathode side, the sink term for oxygen is given by [18, 19];

$$S_{O_2} = -\frac{M_{O_2}}{4F} i_c \quad (17)$$

where M is molecular weight (kg/mole), F is Faraday's constant = 96487 (C/mole), i is local current density (A/m²).

Whereas the sink term for hydrogen is specified as;

$$S_{H_2} = -\frac{M_{H_2}}{2F} i_a \quad (18)$$

The production of water is modelled as a source terms, and hence can be written as;

$$S_{H_2O} = \frac{M_{H_2O}}{2F} i_c \quad (19)$$

The generation of heat in the cell is due to entropy changes as well as irreversibilities due to the activation overpotential [20];

$$\dot{q} = \left[\frac{T(-\Delta s)}{n_e F} + \eta_{act} \right] i \quad (20)$$

where η_{act} is activation over potential (V), n_e is number of electrons transfer, ΔS is entropy change of cathode side reaction.

The local current density distribution in the catalyst layers is modelled by the Butler-Volmer equation [21, 22];

$$i_c = i_{o,c}^{ref} \left(\frac{C_{O_2}}{C_{O_2}^{ref}} \right) \left[\exp\left(\frac{\alpha_a F}{RT} \eta_{act,c} \right) + \exp\left(-\frac{\alpha_c F}{RT} \eta_{act,c} \right) \right] \quad (21)$$

$$i_a = i_{o,a}^{ref} \left(\frac{C_{H_2}}{C_{H_2}^{ref}} \right)^{1/2} \left[\exp\left(\frac{\alpha_a F}{RT} \eta_{act,a} \right) + \exp\left(-\frac{\alpha_c F}{RT} \eta_{act,a} \right) \right] \quad (22)$$

where C_{H_2} is local hydrogen concentration (mole/m³), $C_{H_2}^{ref}$ is reference hydrogen concentration (mole/m³), C_{O_2} is local oxygen concentration (mole/m³), $C_{O_2}^{ref}$ is reference oxygen concentration (mole/m³), C_p is specific heat capacity [J/(kg·K)], D is diffusion coefficient (m²/s), $i_{o,a}^{ref}$ is anode reference exchange current density, $i_{o,c}^{ref}$ is cathode reference exchange current density, R is universal gas constant (=8.314 J/(mole·K)), s is specific entropy [J/(mole·K)], α_a is charge transfer coefficient, anode side, and α_c is charge transfer coefficient, cathode side.

2.2.4 Membrane

The balance between the electro-osmotic drag of water from anode to cathode and back diffusion from cathode to anode yields the net water flux through the membrane [23];

$$N_w = n_d M_{H_2O} \frac{i}{F} - \nabla \cdot (\rho D_w \nabla c_w) \quad (23)$$

where N_w is net water flux across the membrane (kg/m²·s), n_d is electro-osmotic drag coefficient.

The water diffusivity in the polymer can be calculated as follow [24];

$$D_W = 1.3 \times 10^{-10} \exp \left[2416 \left(\frac{1}{303} - \frac{1}{T} \right) \right] \quad (24)$$

The variable c_w represents the number of water molecules per sulfonic acid group (i.e. mol H_2O /equivalent SO_3^-). The water content in the electrolyte phase is related to water vapour activity via [25, 26];

$$\begin{aligned} c_w &= 0.043 + 17.81a - 39.85a^2 + 36.0a^3 & (0 < a \leq 1) \\ c_w &= 14.0 + 1.4(a - 1) & (1 < a \leq 3) \\ c_w &= 16.8 & (a \geq 3) \end{aligned} \quad (25)$$

The water vapour activity given by;

$$a = \frac{x_W P}{P_{sat}} \quad (26)$$

Heat transfer in the membrane is governed by [27];

$$\nabla \cdot (k_{mem} \cdot \nabla T) = 0 \quad (27)$$

where k_{mem} is membrane thermal conductivity [W/(m·K)].

The potential loss in the membrane is due to resistance to proton transport across membrane, and is governed by;

$$\nabla \cdot (\lambda_m \nabla \phi) = 0 \quad (28)$$

where λ_m is membrane ionic conductivity (S/m).

2.2.5 Stresses in fuel cell components

Assuming linear response within the elastic region, the isotropic Hooke's law is used to determine the stress tensor.

$$\Omega = \mathbf{G} \cdot \pi \quad (29)$$

where \mathbf{G} is the constitutive matrix, π is the strain.

Using hygrothermoelasticity theory, the effects of temperature and moisture as well as the mechanical forces on the behaviour of elastic bodies have been addressed. In the present work, the total strain tensor is determined using the same expression of Tang et al. [11];

$$\pi = \pi^M + \pi^T + \pi^S \quad (30)$$

where, π^M is the contribution from the mechanical forces and π^T , π^S are the thermal and swelling induced strains, respectively.

The thermal strains resulting from a change in temperature of an unconstrained isotropic volume are given by;

$$\pi^T = \wp (T - T_{Ref}) \quad (31)$$

where \wp is thermal expansion (1/K).

Similarly, the swelling strains caused by moisture uptake are given by;

$$\pi^S = \tilde{\lambda}_{mem} (\mathfrak{R} - \mathfrak{R}_{Ref}) \quad (32)$$

where $\tilde{\lambda}_{mem}$ is the membrane humidity swelling-expansion tensor (1/%), \mathfrak{R} is the relative humidity (%).

The initial conditions corresponding to zero stress-state are defined; all components of the cell stack are set to reference temperature 20 C, and relative humidity 35% (corresponding to the assembly conditions) [11, 28]. In addition, a constant pressure of (1 MPa) is applied on the upper surface of cathode, corresponding to a case where the fuel cell is equipped with the o-ring cathode current collectors to control the clamping force.

3. Results and discussion

The governing equations were discretized using a finite volume method and solved using a multi-physics general-purpose computational fluid dynamics code. Stringent numerical tests were performed to ensure that the solutions were independent of the grid size. A computational quadratic finer mesh consisting of a

total of 29482 nodes and 130082 meshes were found to provide sufficient spatial resolution (Figure 2). The coupled set of equations was solved iteratively, and the solution was considered to be convergent when the relative error in each field between two consecutive iterations was less than 1.0×10^{-6} . The calculations presented here have all been obtained on a Pentium IV PC (3 GHz, 2GB RAM) using Windows XP operating system.

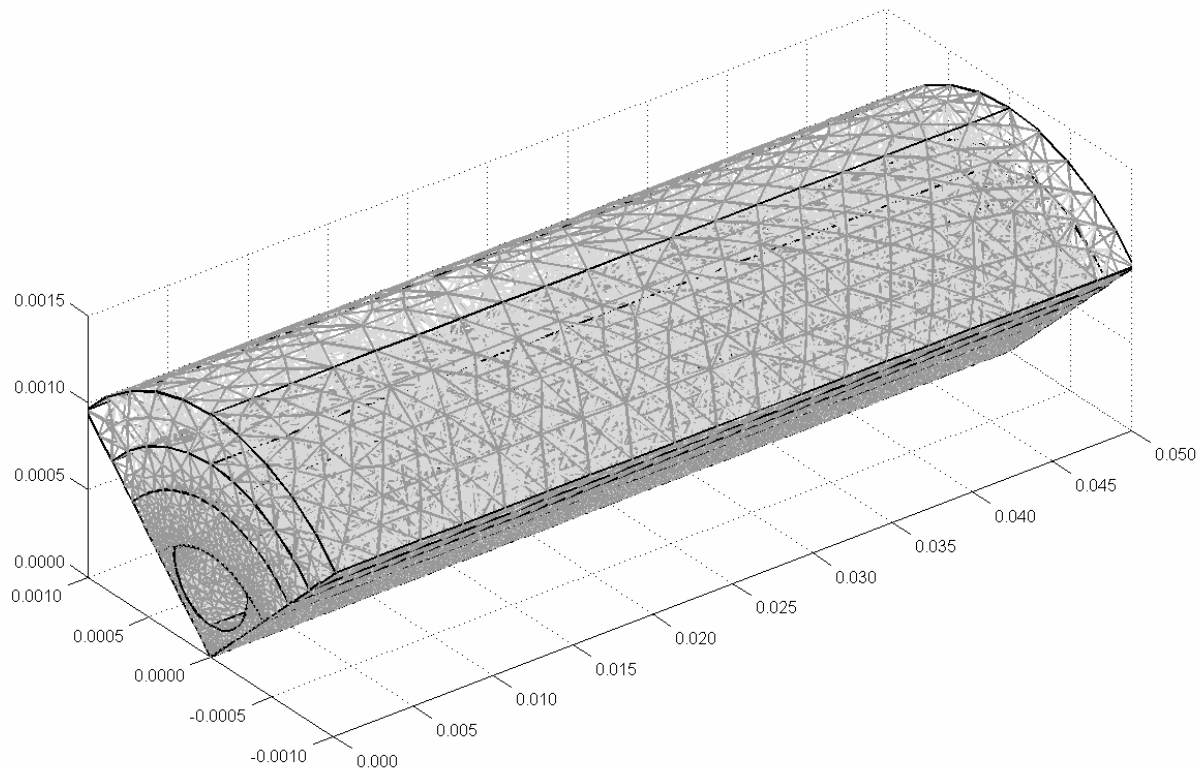


Figure 2. Computational mesh of a tubular-shaped ambient air-breathing PEM micro fuel cell (quadratic)

The values of the electrochemical transport parameters and the material properties used in this model are listed in Table 1. The geometric and the base case operating conditions are listed in Table 2. It is important to note that because this model accounts for all major transport processes and the modelling domain comprises all the elements of a complete cell, no parameters needed to be adjusted in order to obtain physical results. Results for the cell operate at nominal current density of 0.4 A/cm^2 is discussed in this section.

Water management is one of the critical operation issues in proton exchange membrane (PEM) fuel cells. Spatially varying concentrations of water in both vapour and liquid form are usual throughout the cell because of varying rates of production and transport. In the membrane, primary transport is through electro-osmotic drag associated with the protonic current in the electrolyte, which results in water transport from anode to cathode; and diffusion associated with water-content gradients in the membrane. One of the main difficulties in managing water in a PEM fuel cell is the conflicting requirements of the membrane and of the catalyst gas diffusion layer. On the cathode side, excessive liquid water may block or flood the pores of the catalyst layer, the gas diffusion layer or even the gas channel, thereby inhibiting or even completely blocking oxygen mass transfer. On the anode side, as water is dragged toward the cathode via electro-osmotic transport, dehumidification of the membrane may occur, resulting in deterioration of protonic conductivity. In the extreme case of complete drying, local burnout of the membrane can result. Figure 3 shows profiles for polymer water content in the membrane for the base case conditions. The influence of electro-osmotic drag and back diffusion are readily apparent from this result.

Table 1. Electrode and membrane parameters for base case operating conditions

Parameter	Sym.	Value	Unit	Ref.
Electrode porosity	ε	0.4	-	[18]
Electrode electronic conductivity	λ_e	100	S/m	[27]
Membrane ionic conductivity	λ_m	17.1223	S/m	[18]
Transfer coefficient, anode side	α_a	0.5	-	[19]
Transfer coefficient, cathode side	α_c	1	-	[22]
Cathode ref. exchange current density	$i_{o,c}^{ref}$	1.8081e-3	A/m^2	[14]
Anode ref. exchange current density	$i_{o,a}^{ref}$	2465.598	A/m^2	[14]
Electrode thermal conductivity	k_{eff}	1.3	$W/m.K$	[16]
Membrane thermal conductivity	k_{mem}	0.455	$W/m.K$	[16]
Electrode hydraulic permeability	kp	1.76e-11	m^2	[21]
Entropy change of cathode side reaction	ΔS	-326.36	$J/mole.K$	[20]
Heat transfer coefficient between solid & gas phase	β	4e6	W/m^3	[17]
Protonic diffusion coefficient	D_{H^+}	4.5e-9	m^2/s	[18]
Fixed-charge concentration	c_f	1200	$mole/m^3$	[18]
Fixed-site charge	z_f	-1	-	[18]
Electro-osmotic drag coefficient	n_d	2.5	-	[23]
Droplet diameter	D_{drop}	1.0×10^{-8}	m	[15]
Condensation constant	C	1.0×10^{-5}	-	[15]
Scaling parameter for evaporation	ϖ	0.01	-	[15]
Electrode Poisson's ratio	\mathfrak{S}_{GDL}	0.25	-	[11]
Membrane Poisson's ratio	\mathfrak{S}_{mem}	0.25	-	[11]
Electrode thermal expansion	\wp_{GDL}	-0.8×10^{-6}	$1/K$	[11]
Membrane thermal expansion	\wp_{mem}	123×10^{-6}	$1/K$	[28]
Electrode Young's modulus	Ψ_{GDL}	1×10^{10}	Pa	[11]
Membrane Young's modulus	Ψ_{mem}	249×10^6	Pa	[28]
Electrode density	ρ_{GDL}	400	kg/m^3	[11]
Membrane density	ρ_{mem}	2000	kg/m^3	[11]
Membrane humidity swelling-expansion tensor	λ_{mem}	23×10^{-4}	$1/\%$	[11]

Table 2. Geometrical and operational parameters for base case conditions

Parameter	Sym.	Value	Unit
Channel length	L	0.05	m
Channel width	W	1e-3	m
Channel height	H	1e-3	m
Land area width	W_{land}	1e-3	m
Gas diffusion layer thickness	δ_{GDL}	0.26e-3	m
Wet membrane thickness (Nafion® 117)	δ_{mem}	0.23e-3	m
Catalyst layer thickness	δ_{CL}	0.0287e-3	m
Hydrogen reference mole fraction	$x_{H_2}^{ref}$	0.84639	-
Oxygen reference mole fraction	$x_{O_2}^{ref}$	0.17774	-
Anode pressure	P_a	3	atm
Cathode pressure	P_c	3	atm
Inlet fuel and air temperature	T_{cell}	353.15	K
Relative humidity of inlet fuel and air	ψ	100	%
Air stoichiometric flow ratio	ξ_c	2	-
Fuel stoichiometric flow ratio	ξ_a	2	-

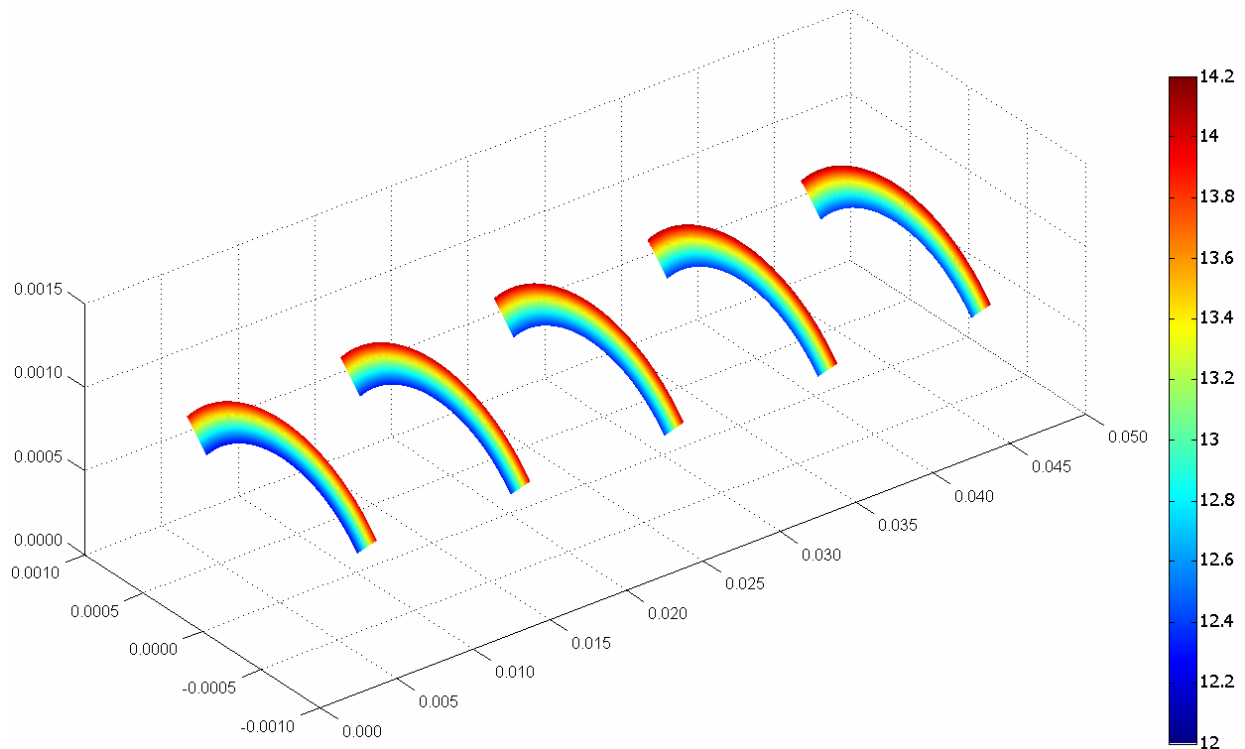


Figure 3. Water content profiles through the MEA

Thermal management is also required to remove the heat produced by the electrochemical reaction in order to prevent drying out of the membrane and excessive thermal stresses that result in rupture of the membrane or mechanical damage in the cell. The small temperature differential between the fuel cell stack and the operating environment make thermal management a challenging problem in PEM fuel cells. The temperature distribution inside the fuel cell has important effects on nearly all transport phenomena, and knowledge of the magnitude of temperature increases due to irreversibilities might help preventing failure. Figure 4 shows the distribution of the temperature inside the cell. The result shows that the increase in temperature can exceed a number of degrees Kelvin near the catalyst layer regions, where the electrochemical activity is highest. The temperature peak appears in the cathode catalyst layer, implying that major heat generation takes place in the region. In general, the temperature at the cathode side is higher than that at the anode side; this is due to the reversible and irreversible entropy production. The durability of proton exchange membranes used in fuel cells is a major factor in the operating lifetime of fuel cell systems. The stresses distribution in the fuel cells is affected by operating point (cell voltage and related current density). The stresses distribution in Membrane-Electrode-Assembly (MEA) and gas diffusion layers that developed during the cell operating can be seen in Figure 5. The total displacement values that occur in the cell and the deformation shape of the cell are also shown in figure 6 and 7 respectively.

Because of the different thermal expansion and swelling coefficients between gas diffusion layers and membrane materials with non-uniform temperature distributions in the cell during operation, hygro-thermal stresses and deformation are introduced. The non-uniform distribution of stress, caused by the temperature gradient in the MEA and gas diffusion layers, induces localized bending stresses, which can contribute to delaminating between the membrane and the gas diffusion layers. The non-uniform distribution of stresses can also contribute to delaminating between the gas diffusion layers and the bipolar plates. These stresses may explain the occurrence of cracks and pinholes in the fuel cells components under steady-state loading during regular cell operation, especially in the high loading conditions.

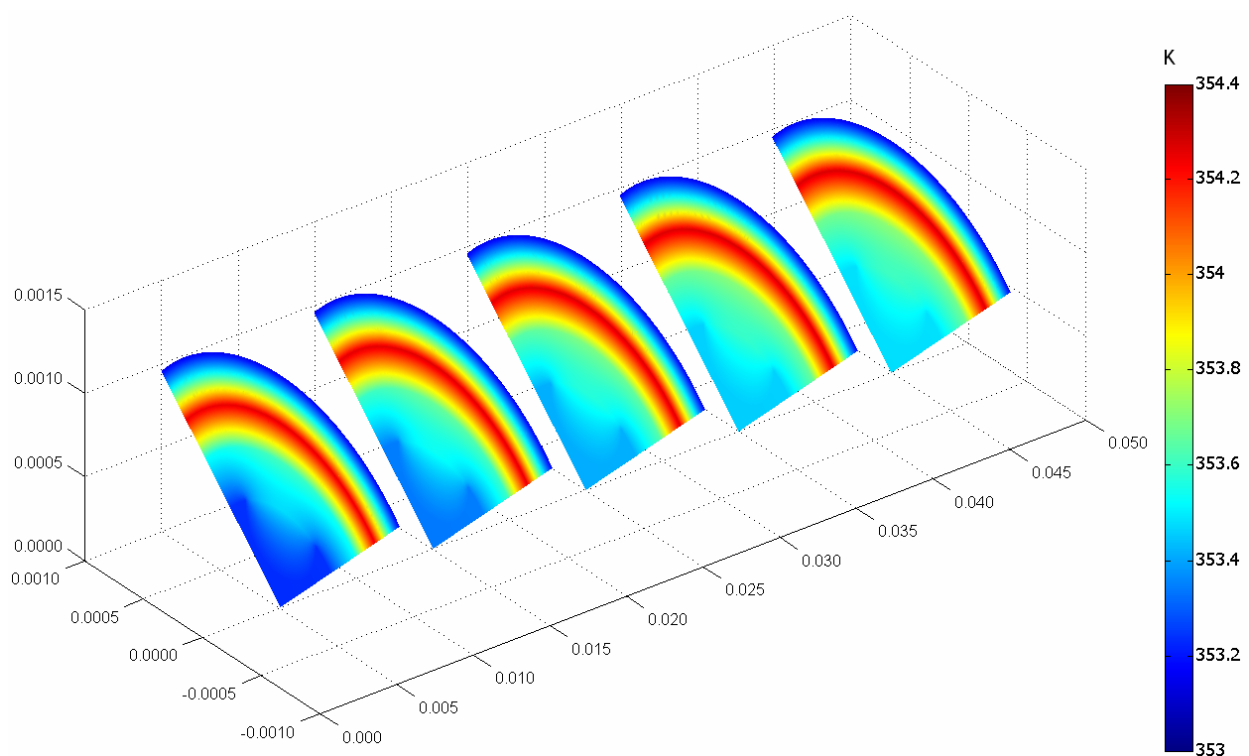


Figure 4. Temperature distribution inside the cell

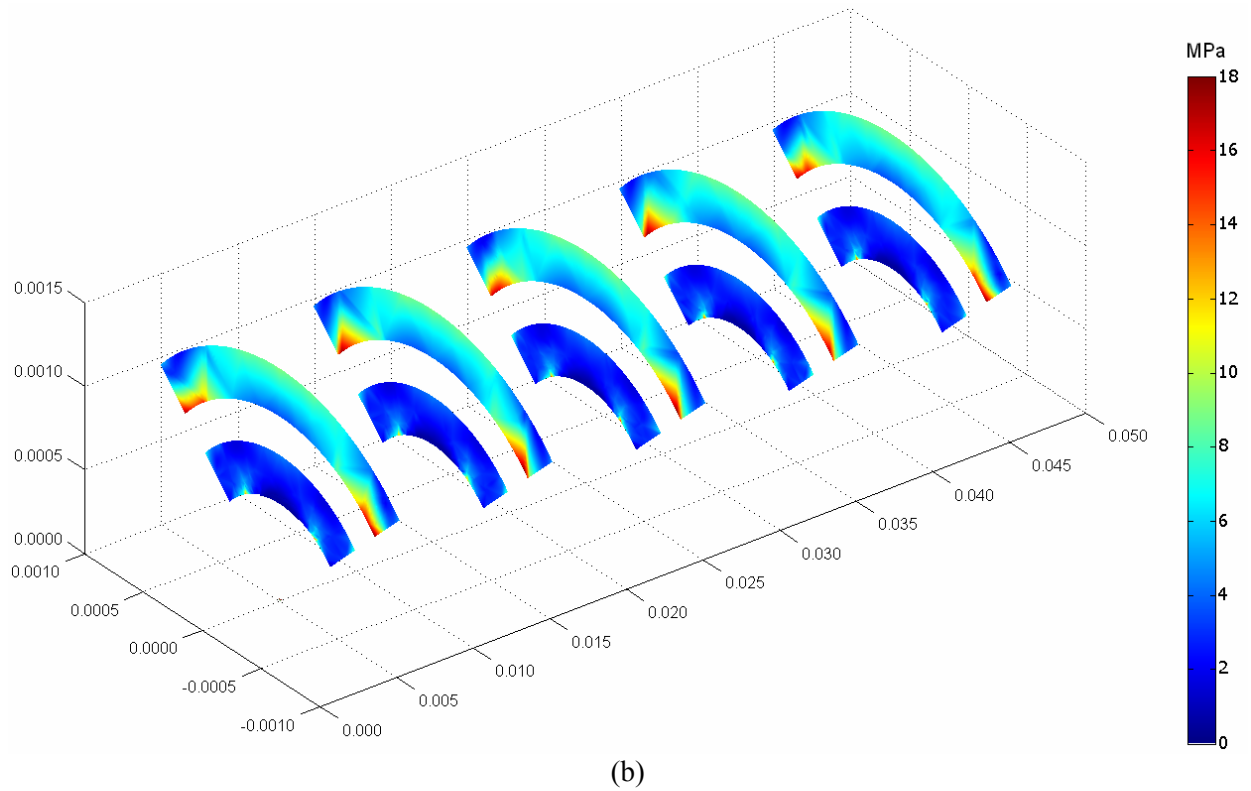
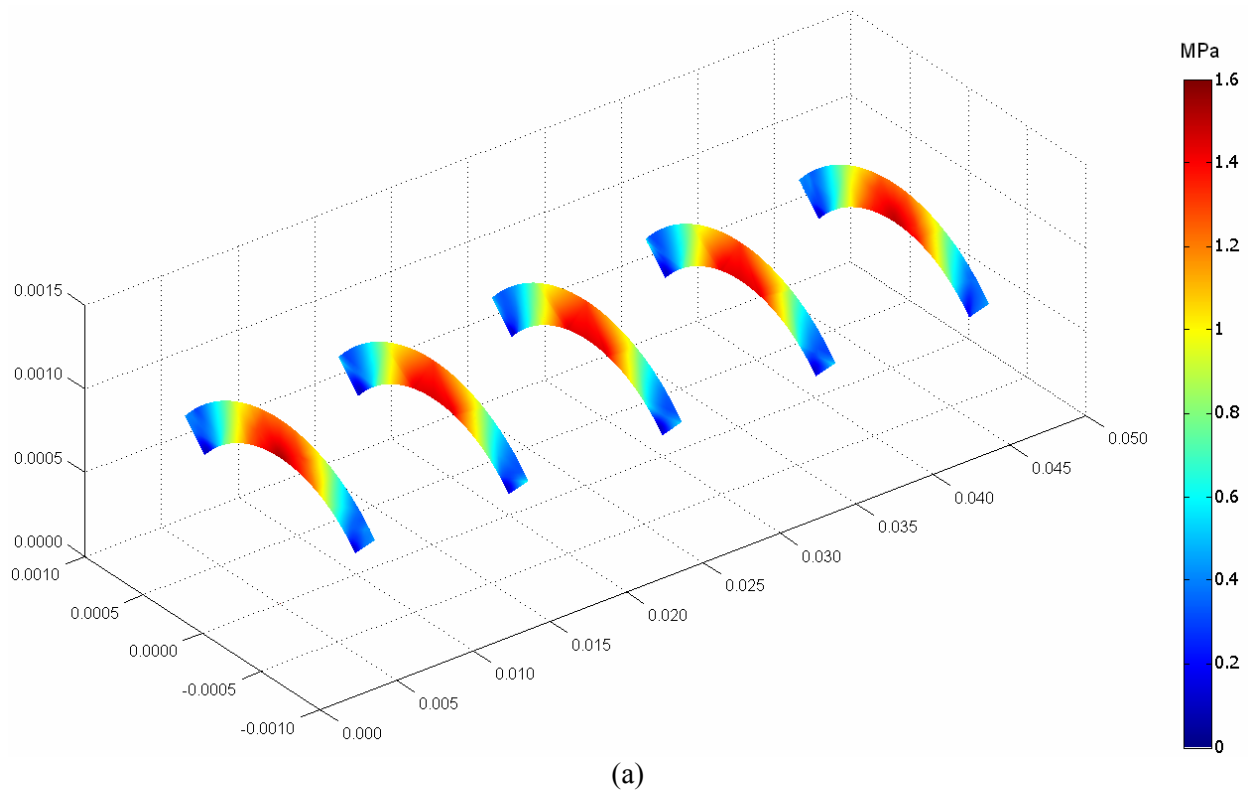


Figure 5. Von Mises stress distribution inside (a) membrane, and (b) gas diffusion layers

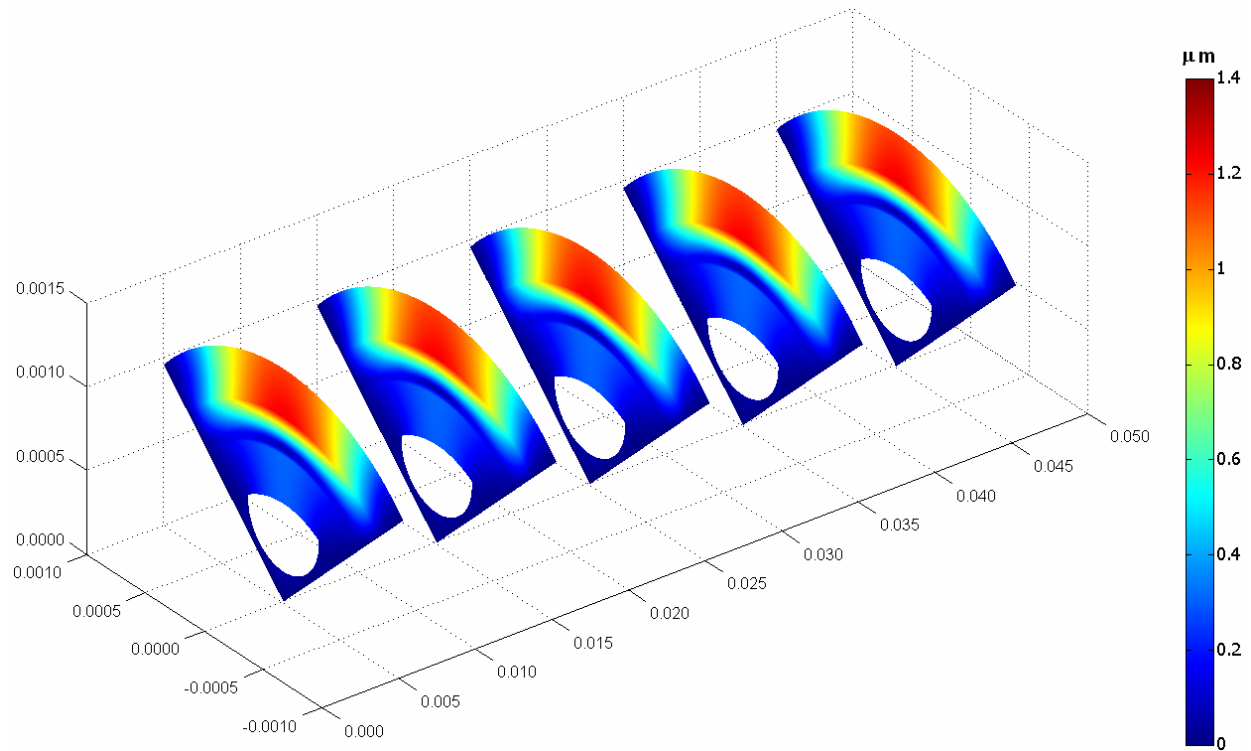


Figure 6. Total displacement distribution inside the cell

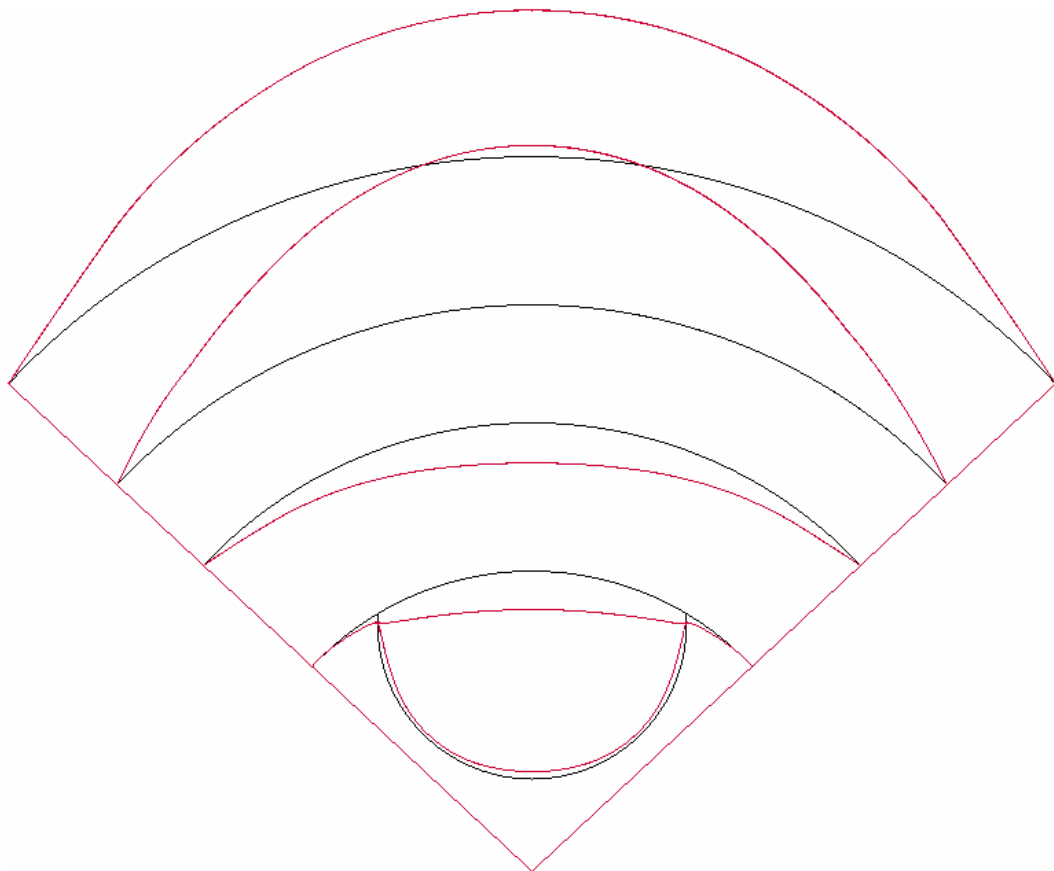


Figure 7. Deformed shape plot (scale enlarged 250 times) for the cell: (black lines) initial conditions (assembly conditions) corresponding to zero stress-state, and (red lines) during regular cell operation

4. Conclusions

A full three-dimensional, multi-phase computational fluid dynamics model of a novel tubular-shaped ambient air-breathing PEM micro fuel cell has been developed to simulate the hygro and thermal stresses in polymer membrane and gas diffusion layers, which developed during the cell operation. This comprehensive model accounts for the major transport phenomena in the cell: convective and diffusive heat and mass transfer, electrode kinetics, transport and phase change mechanism of water, and potential fields. The behaviour of the fuel cell during operation has been studied and investigated under real cell operating conditions. The results show that the non-uniform distribution of stresses, caused by the temperature gradient and moisture change in the cell, induces localized bending stresses, which can contribute to delaminating between the membrane and the gas diffusion layers. The non-uniform distribution of stresses can also contribute to delaminating between the gas diffusion layers and the current collectors. These stresses may explain the occurrence of cracks and pinholes in the fuel cells components under steady-state loading during regular cell operation, especially in the high loading conditions.

References

- [1] Wang Y. and Ouyang M. Three-dimensional heat and mass transfer analysis in an air-breathing proton exchange membrane fuel cell. *J. Power Sources*, 2007, 164(2), 721-729.
- [2] Litster S. and Djilali N. Mathematical modelling of ambient air-breathing fuel cells for portable devices. *Electrochimica Acta J.* 2007, 52(11), 3849-3862.
- [3] Hwang J.J., Wu S.D., Pen R.G., Chen P.Y., and Chao C.H. Mass/electron co-transport in an air-breathing cathode of a PEM fuel cell. *J. Power Sources*, 2006, 160(1), 18-26.
- [4] Zhang Y. and Pitchumani R. Numerical studies on an air-breathing proton exchange membrane (PEM) fuel cell. *Int. J. Heat and Mass Transfer*, 2007, 50(23-24), 4698-4712.
- [5] Beuscher, U., Cleghorn, S.J.C., Johnson, W.B. Challenges for PEM fuel cell membranes. *Int. J. Energy Research* 2005; 29(12): 1103-1112.
- [6] Gode, P., Itonen, J., Strandroth, A., Ericson, H., Lindbergh, G., Paronen, M., Sundholm, F., Sundholm, G., Walsby, N. Membrane Durability in a PEM Fuel Cell Studied Using PVDF Based Radiation Grafted Membranes Fuel Cells. *Fuel Cells* 2003; 3(1-2): 21-27.
- [7] Xie, J., Wood, D.L., Wayne, D.M., Zawodzinski, T., Borup, R.L. Durability of Polymer Electrolyte Fuel Cells at High Humidity Conditions. *J. Electrochem. Soc.* 2005; 152(1): A104-A113.
- [8] Stanic, V., Hoberech, M. Mechanical of pin-hole formation in membrane electrode assemblies for PEM fuel cells. *Proceedings of the Fourth International Symposium on Proton Conducting Membrane Fuel Cells*, Coral 5, Level 6, Mid Pacific Conference Centre; 2004.
- [9] Tang, Y., Karlsson, A.M., Santare, M.H., Gilbert, M., Cleghorn, S., Johnson, W.B. An experimental investigation of humidity and temperature effects on the mechanical properties of perfluorosulfonic acid membrane. *J. Materials Science and Engineering* 2006; 425(1-2): 297-304.
- [10] Webber, A., Newman, J. A Theoretical Study of Membrane Constraint in Polymer-Electrolyte Fuel Cell. *AIChE J.* 2004; 50(12): 3215-3226.
- [11] Tang, Y., Santare, M.H., Karlsson, A.M., Cleghorn, S., Johnson, W.B. Stresses in Proton Exchange Membranes Due to Hygro-Thermal Loading, *J.FuelCell Sci.&Tech. ASME* 2006; 3(5); 119-124.
- [12] Kusoglu, A., Karlsson, A., Santare, M., Cleghorn, S., Johnson, W. Mechanical response of fuel cell membranes subjected to a hygro-thermal cycle. *J. Power Sources* 2006; 161(2): 987-996.
- [13] Fuller E.N., Schettler P.D., Giddings J.C. A new method for prediction of binary gas-phase diffusion coefficients. *Ind. Eng. Chem.* 1966; 58(5): 18-27.
- [14] Berning T., Djilali N. Three-dimensional computational analysis of transport phenomenon in a PEM fuel cell-a parametric study. *J. Power Sources* 2003; 124(2): 440-452.
- [15] Berning T., Djilali N. A 3D, multi-phase, multicomponent model of the cathode and anode of a PEM fuel cell. *J. Electrochem. Soc.* 2003; 150(12): A1589-A1598.
- [16] Nguyen P.T., Berning T., Djilali N. Computational model of a PEM fuel cell with serpentine gas flow channels. *J. Power Sources* 2004; 130(1-2): 149-157.
- [17] Berning T., Lu D.M., Djilali N. Three-dimensional computational analysis of transport phenomena in a PEM fuel cell. *J. Power Sources* 2002; 106(1-2): 284-294.

- [18] Bernadi D.M., Verbrugge M.W. A mathematical model of the solid-polymer-electrolyte fuel cell. *J. Electrochem. Soc.* 1992; 139(9): 2477-2491.
- [19] Gurau V., Liu H., Kakac S. Two-dimensional model for proton exchange membrane fuel cells. *AIChE Journal* 1998; 44(11): 2410–2422.
- [20] Lampinen M.J., Fomino M. Analysis of free energy and entropy changes for half-cell reactions. *J. Electrochem. Soc.* 1993; 140(12): 3537–3546.
- [21] Wang L., Husar A., Zhou T., Liu H. A parametric study of PEM fuel cell performances. *Int. J. Hydrogen Energy* 2003; 28(11): 1263– 1272.
- [22] Parthasarathy A., Srinivasan S., Appleby J.A., Martin C.R. Pressure dependence of the oxygen reduction reaction at the platinum microelectrode/nafion interface: electrode kinetics and mass transport. *J. Electrochem. Soc.* 1992; 139(10): 2856–2862.
- [23] Springer T.E., Zawodzinski T.A., Gottesfeld, S. Polymer electrolyte fuel cell model. *J. Electrochem. Soc.* 1991; 138(8): 2334-2342.
- [24] Siegel N.P., Ellis M.W., Nelson D.J., von Spakovsky M.R. A two-dimensional computational model of a PEMFC with liquid water transport. *J. Power Sources* 2004; 128(2): 173–184.
- [25] Hu M., Gu A., Wang M., Zhu X., Yu L. Three dimensional, two phase flow mathematical model for PEM fuel cell. Part I. Model development. *Energy Conversion Manage* 2004; 45(11):1861–1882.
- [26] Hu M., Gu A., Wang M., Zhu X., Yu L. Three dimensional, two phase flow mathematical model for PEM fuel cell. Part II. Analysis and discussion of the internal transport mechanisms. *Energy Conversion Manage* 2004; 45(11-12): 1883–1916.
- [27] Sivertsen B.R., Djilali N. CFD based modelling of proton exchange membrane fuel cells. *J. Power Sources* 2005; 141(1): 65-78.
- [28] Product Information DuPont™ Nafion® PFSA Membranes N-112, NE-1135, N-115, N-117, NE-1110 Perfluorosulfonic Acid Polymer. NAE101; 2005.